In Vivo Characterization of Neurophysiological Diversity in the Lateral Supramammillary Nucleus during Hippocampal Sharp-wave Ripples of Adult Rats

Ana F Vicente, Andrea Slézia, Antoine Ghestem, Christophe Bernard, Pascale P. Quilichini

In Vivo Characterization of Neurophysiological Diversity in the Lateral Supramammillary Nucleus during Hippocampal Sharp-wave Ripples of Adult Rats

Ana F. Vicente,* Andrea Slézia, Antoine Ghestem, Christophe Bernard*[γ] and Pascale P. Quilichini*[γ]

Aix Marseille Univ, INSERM, INS, Inst Neurosci Syst, Marseille, France

*Corresponding authors.

E-mail addresses: ana-maria.fernandez-vicente@univ-amu.fr (A. F. Vicente), christophe.bernard@univ-amu.fr (C. Bernard), pascale.quilichini@univ-amu.fr (P. P. Quilichini). [γ] Equally last authors.

Abstract—The extent of the networks that control the genesis and modulation of hippocampal sharp-wave ripples (SPW-Rs), which are involved in memory consolidation, remains incompletely understood. Here, we performed a detailed in vivo analysis of single cell firing in the lateral supramammillary nucleus (lSuM) during theta and slow oscillations, including SPW-Rs, in anesthetized rats. We classified neurons as SPW-R-active and SPW-R unchanged according to whether or not they increased their firing during SPW-Rs. We show that lSuM SPW-R active neurons increase their firing prior to SPW-Rs peak power and prior to hippocampal excitatory cell activation. Moreover, lSuM SPW-R-active neurons show increased firing activity during theta and slow oscillations as compared to unchanged neurons. These results suggest that a sub-population of lSuM neurons can interact with the hippocampus during SPW-Rs, raising the possibility that the lSuM may modulate memory consolidation.

Key words: hippocampus, lateral supramammillary nucleus, sharp-wave ripple, firing, theta, slow oscillation.

INTRODUCTION

Sharp-wave ripples (SPW-Rs) consist of a distinctive activity pattern of the hippocampal local field potential (LFP) in the CA1 region that can occur during sleep and awake immobility (Buzsáki, 2015). This phenomenon involves two components: a negative deflection called the sharp-wave and a fast oscillation (150–250 Hz) called the ripple. Several studies suggest that SPW-Rs play a key role in the transfer of information between the hippocampus (HPC) and the neocortex (Diekelmann and Born, 2010; Maingret et al., 2016). The mechanisms underlying the genesis of SPW-Rs remain mostly unknown. They appear to be an emergent property of neuronal networks, which could involve different brain regions, as for gamma oscillations (Sohal and Huguenard, 2005; Buzsáki and Schomburg, 2015). Several studies have shown the involvement of the CA1/ CA3 subfields of the HPC in SPW-Rs (Buzsáki, 2015).

CA3 synchronous bursts depolarize CA1 pyramidal neurons in *stratum radiatum*, resulting in a negative LFP deflection (sharp waves) (Buzsáki et al., 1983). This synchronous activity triggers the firing of CA1 interneurons at a high frequency (Csicsvari et al., 2000), which, together with CA3 activation result in fast field oscillations known as ripples (Ylinen et al., 1995).

A change in firing frequency of neurons around SPWRs is generally considered as a marker of their involvement in SPW-R genesis and/or in memory consolidation process. For example, HPC neurons increase their firing during SPW-R events in sleep, reflecting neuronal patterns associated with previous experiences (Lee and Wilson, 2002). Oliva et al. (2016) demonstrated that CA2 neurons' firing precedes the activation of CA3 and CA1 during SPW-Rs, suggesting a prominent role of CA2 region in SPW-R genesis. In line with a distributed network phenomenon, several studies have looked at the interaction between SPW-Rs and different subcortical areas (Pennartz, 2004; Girardeau et al., 2017). A typical example is the septum, whose neurons increase or decrease their discharge probability during SPW-Rs (Dragoi et al., 1999; Unal et al., 2018). A clear understanding of the mechanisms underlying the genesis of SPW-Rs may require the identification of all the structures that can control or modulate HPC SPW-Rs.

The goal of the present study is to determine whether the supramammillary nucleus (SuM) is part of the network that can generate or modulate SPW-Rs, using as a marker a change in the firing activity of SuM neurons around the time of occurrence of HPC SPW-Rs. The SuM is a hypothalamic region divided into medial and lateral parts (lSuM) according to their respective different connections to the HPC (Pan and McNaughton, 2004). The lSuM sends projections to the dentate gyrus (DG) throughout both dorsal and ventral HPC, to dorsal CA2/ CA3 (Vertes, 1992), and is reciprocally connected with the septal complex (Leranth and Kiss, 1996; Borhegyi et al., 1998). Electrophysiological studies of the SuM showed its role in theta oscillations (THETA) due to its connections with the septum, which is considered a THETA pacemaker (Pignatelli et al., 2012). Kocsis and Vertes (1994) described SuM neurons firing rhythmically with THETA recorded in dorsal HPC. Moreover, Kirk and McNaughton (1993) showed that the pharmacological blockade of the medial SuM results in a decrease in frequency and amplitude of hippocampal THETA. These results suggest the involvement of the SuM in THETA modulation. However, no studies have described the activity of the SuM during slow oscillations periods (SO) and its possible role in SPW-Rs. The connectivity of the SuM with both HPC and septum (Borhegyi et al., 1998; Kiss et al., 2000) provides a morphological substrate for the potential involvement of the lSuM in the control/genesis of SPW-Rs.

To examine this possible involvement during SO, rats were implanted with silicone probes into dorsal CA1/CA2/ CA3 HPC, DG and lSuM. This procedure allowed us to record LFP and firing activity simultaneously during both THETA and SO under anesthesia. We found a population of lSuM neurons increasing its firing around hippocampal SPW-Rs, which we called ''SPW-R-active neurons''. Additionally, these neurons showed distinct firing properties comparing to those lSuM neurons showing no firing increases during SPW-Rs.

EXPERIMENTAL PROCEDURES

Ethical approval

All experiments were performed in accordance with AixMarseille Université and Inserm Institutional Animal Care and Use Committee guidelines. The protocol was approved by the French Ministry of National Education, Superior Teaching and Research (approval number: 01451-02). All surgical procedures were performed under anesthesia. All experiments described here comply with the policies and regulations described in Grundy (2015).

Animal surgery

Seven Wistar Han IGS male rats (Charles Rivers) were used in this study. Animals were housed for at least 7 days upon arrival in groups of 2, to avoid social isolation-induced stress (Manouze et al., 2019) in a temperature (22 ± 1 C) and humidity (60–70%) controlled facility on a 12 h light–dark cycle (07.00-19.00 h) with food and water available ad libitum. Animals were anesthetized with urethane (1.5 g/kg, i.p.) and ketamine/xylazine (20 and 2 mg/kg, i.m.) with additional doses of ketamine/ xylazine (2 and 0.2 mg/kg) when needed during the electrophysiological recordings. Animal breathing, heart rate, pulse distension, and arterial oxygen saturation were monitored with a pulse oximeter (MouseOX; StarrLife Science) during the whole experiment. The animal was placed in a stereotaxic frame; and its head was exposed. Two stainless-steel screws were implanted into the skull above the cerebellum, serving as reference and ground electrodes. Two craniotomies were performed to target the dorsal HPC (coordinates from bregma for animals A–C: AP 3 mm, ML 2.4 mm, DV 2.4 mm, with 20 angle; for animals D–E: AP 2.5 mm, ML 3 mm, DV 2.4 mm, with 20 angle; for animals F–G: AP 3

mm, ML 4.2, DV 2.4 mm, with 20 angle) and the lSuM (coordinates from bregma for animals A–E: AP 4.44 mm, ML 2 mm, DV 8.6 mm, with 10 angle). We performed simultaneous recordings with 32-site silicon probes (Neuronexus Technologies, Cambridge Neurotech) of the following areas: CA1, DG, and lSuM for animals A–E, CA1 and CA2 for animal F, and CA1 and CA3 for animal G.

The lSuM was recorded with an H32-Edge-10 mm-20 mm-177 probe in animals A–E, and the HPC was recorded with the following probes: an H32-Poly2-5 mm-25 mm-177 probe for animal A, a linear H32-6 mm50 mm-177 probe for animal B, a linear H32-10 mm100 mm-177 probe for animal C, and a two-shank linear H162-10 mm-100 mm-177 probe for animals E and F, H32Edge-10 mm-20 mm-177 probe for animals F–G, and Cambridge NeuroTech E1-2shanks20mm-177 probe for animals F–G. Table S1 summarizes the number of neurons recorded in each animal.

All silicon probes were mounted on individual stereotaxic manipulators and lowered manually for HPC and with a motorized descender (IVM, Scientifica) for lSuM. The final position of the probes was adjusted according to the presence of unit activity in cell body layers and the presence of ripples (100–200) Hz in CA1 *stratum pyramidale*.

Electrophysiological recordings and initial analysis

Extracellular signal was amplified (1000), bandpass filtered (1 Hz to 5 kHz) and acquired continuously at 32 kHz with a Digital Lynx (NeuraLynx) at 16-bit resolution. Raw data were preprocessed using NEUROSUITE (Hazan et al., 2006; http://neurosuite.sourceforge.net/; RRID: SCR_008020). The signal was downsampled to 1250 Hz for the LFP analysis. Spike sorting was performed automatically, using KLUSTAKWIK (Harris et al., 2000; http://klustakwik.sourceforge. net/; RRID: SCR_014480), followed by a manual adjustment of the clusters, with the help of auto-correlogram, cross-correlogram, and spike wave-form similarity matrix with KLUSTERS software (Hazan et al., 2006; RRID: SCR_008020). Only units showing a clear refractory period and a well-defined cluster were included for posterior analysis. THETA and SO periods were identified for each recording. LFP THETA or SO epochs were visually selected from the ratios of the whitened power in the THETA band (3–6 Hz) and the power of the neighboring bands (1–3, and 7–14 Hz) of CA1 pyramidal layer, and from the ratio of the whitened power in the SO band (0.5–2 Hz) of CA1 pyramidal layer, respectively. We used a 3–6 Hz range because the mean peak of THETA in the CA1 pyramidal layer was 4.66 ± 0.43 Hz (n = 7 animals). This procedure was assisted by visual inspection of the raw traces (Quilichini et al., 2010).

Single unit identification

Units were identified as lSuM neurons by determining the histological reconstruction of the recording silicon probes tracks, the approximate location of their somata relative to the recording sites, and the known distances of the recorded sites. CA2 region was identified from histological sections by the

thicker pyramidal layer and sparser cell bodies compared to CA1, and validated by immunolabeling by the CA2 specific marker PCP4. Hippocampal putative excitatory neurons and interneurons were separated on the basis of their autocorrelograms, firing rates, and waveforms features, assisted by monosynaptic excitatory and inhibitory interactions between pairs of neurons simultaneously recorded reflected on the cross-correlograms (Csicsvari et al., 1998; Barthó et al., 2004).

Histological analysis

At the end of the recording, the animals were injected with a lethal dose of pentobarbital Na (150 mg/kg, i.p.) and perfused intracardially with 4% paraformaldehyde solution in 0.12 M phosphate buffer (PB), pH 7.4. The brains were removed and post-fixed at 4 C overnight. They were then rinsed in PB and sliced into 60-mm-thick coronal sections by a Vibratome. The position of the electrodes was revealed by the presence of DiIC18(3) (Interchim), which was applied on the back of the electrodes before insertion and confirmed histologically on fluorescent Nissl-stained sections (Neuro-Trace 500/5225 Green Fluorescent Nissl Stain, Invitrogen). Immunolabeling for the CA2 region specific marker PCP4 was performed for animals F and G. Sections were washed 3 times in KPBS-Triton 0.02%, then blocked with 3% bovine serum albumin in KPBS-Triton and incubated overnight at room temperature with the primary antibody solution (rabbit anti-PCP4, 1/300, Sigma, HPA005792). Sections were washed 3 times in KPBS-Triton 0.3% and incubated for 2 hours at room temperature with goat anti-rabbit Alexa Fluor 488 1/200, Jackson Immunoresearch A-11008). Sections were then mounted on glass slides with fluorescence medium (Fluoromount-G, ThermoFisher). Only experiments with the appropriate position of the electrodes were used for analysis.

SPW-Rs analysis

SPW-Rs were detected during SO periods with RippleLab (Navarrete et al., 2016) independently on each recording. LFP corresponding to the hippocampal *stratum pyramidale* was digitally band-pass filtered 80–250 Hz, and the power (root-mean-square) of the filtered signal was calculated. The mean and SD of the power signal were calculated to determine the detection threshold. Oscillatory epochs with a power of 5 or more SD above the mean were detected. The beginning and the end of oscillatory epochs were marked at points where the power fell <0.5 SD. Short events (<15 ms) were discarded and adjacent events (gap >15 ms) were merged. All events were visually confirmed to avoid false positives. Only those events simultaneously detected with a sharp-wave in the *stratum radiatum* were kept for further analysis, confirmed by the negative correlation between the whitened signal of each ripple event and its corresponding sharp-wave, assisted by visual inspection. Inter-SPW-Rs periods were defined as SO periods by excluding SPWRs times.

Correlation between unit firing and SPW-Rs

Spikes of each neuron detected in a 200 ms window centered on the peak of each ripple power were binned (5 ms time bin) to construct ripple cross-correlograms. To assess the significance of these cross-correlograms a nonparametric significance test based on jittering was used (Fujisawa et al., 2008; Amarasingham et al., 2012; Ferraris et al., 2018). Surrogate tests (n = 1000 surrogates, 100 ms window interval) were applied to set the 95% upper and lower confidence intervals. Then, the cross-correlograms were constructed for the surrogate datasets as a function of latency across the interval [100, + 100] ms. Pointwise lines at 99% acceptance level were constructed for the cross-correlograms from the maximum and minimum of each jitter surrogate cross-correlogram across the interval [100, +100] ms. Neurons crossing the upper or lower pointwise lines for at least 3 consecutive bins were considered as positively or negatively correlated with SPW-Rs, respectively.

Raster plots were constructed for each neuron by collecting the spikes detected in a 400 ms window centered on the peak of each ripple power. Spikes were binned (1 ms time bin) and cross-correlograms were constructed. The cross-correlograms were z-scored and smoothed using a Gaussian kernel (SD = 5 ms) to construct the raster plots. The latency peak firing during SPW-R for each neuron was based on these z-scored smoothed cross-correlograms. For each type of neuron (excitatory, interneurons and lSuM neurons), all z-scored smoothed cross-correlograms were pooled and mean and SD curves calculated.

Participation probability was calculated for each neuron defined as the number of SPW-Rs in which a neuron fires divided by the total number of SPW-Rs (Oliva et al., 2016).

Firing properties analysis

Firing properties were analyzed for each neuron to determine differences among the types of neurons for both THETA and SO.

Bursting was analyzed by calculating a burst index for each neuron obtained from the autocorrelogram of each neuron (1 ms bin) by subtracting the mean frequency between 40 and 50 ms (baseline) from the maximum frequency between 0-10 ms. Positive values were normalized to the peak frequency and negative values were normalized to the baseline to obtain indices ranging from 1 to 1. Indices 0.6 indicated bursting. Intra-burst frequency was defined as the maximum frequency between 0-10 ms and was calculated for those neurons showing a burst index 0.6 (Royer et al., 2012; Ferraris et al., 2018).

We also analyzed the firing properties for every SuM neuron during SPW-R and inter-SPW-R periods (Katona et al., 2014; Unal et al., 2018). SPW-R firing rate was calculated by summing all spikes during the detected SPWRs and dividing the result by the sum of durations of all SPW-Rs. To calculate firing rate for inter-SPW-R epochs, a set of 1000 surrogates time windows (surrogate SPWRs) was created for every SPW-R. Surrogate SPW-Rs were restricted to SO periods by excluding SPW-R periods. The firing rate for every surrogate SPW-R was calculated and its average was derived for every neuron. The same procedure was followed to calculate burst index and intra-burst frequency.

Autocorrelograms (1 ms bin size) were built for every neuron for THETA and SO periods.

Statistics

All results reported are based on estimation statistics which provide the effect size and the 95% confidence interval (CI) of the median difference between two groups. We directly introduced the raw data in https:// www.estimationstats.com/ and downloaded the results and graphs. The median difference for two comparisons is shown with Cumming estimation plot. The raw data is plotted on the upper axes. For each group, summary measurements (mean ± standard deviation) are shown as gapped lines. Each median difference is plotted on the lower axes as a bootstrap sampling distribution. Five thousand bootstrap samples were taken; the confidence interval was bias corrected. Median differences are depicted as dots; 95% confidence intervals are indicated by the ends of the vertical error bars. In order to measure the effect size, we used the difference between medians. We also provide P value(s) the likelihood(s) of observing the effect size(s), if the null hypothesis of zero difference is true, using the test mentioned in the text. If 95% CI includes 0, differences are considered as non-significant. P values are also provided. In the case 95% CI includes 0 and p-values is lower than 0.05, differences are also considered as nonsignificant. We used nonparametric testing in most cases: two-sided paired testing Wilcoxon's signed-rank test for paired groups and two-sided Kruskal–Wallis test for unpaired groups and provided the median value for each group. Hartigans' Dip test was used to verify if the distribution of firing parameters was significantly bimodal (p < 0.05).

To establish the THETA and SO modulation of units, the phase of the hippocampal oscillations was determined from the filtered LFP in the 3–6 Hz and 0.5–2 Hz ranges, respectively. The instantaneous phase was computed as the angle of the Hilbert transform. Using linear interpolation, a value of phase was assigned to each spike. The modulation of lSuM spikes was determined by Rayleigh circular statistics. P values <0.05 were considered significant. Because the spike-phase estimation is influenced by the number of spikes (Ito et al., 2018), we performed a bootstrap resampling procedure. We equalized the number of spikes between the two groups comparisons (SPW-R-active and SPW-R-unchanged neurons) by randomly subsampling the spikes from the bigger group and calculated phase preference on this subsampling. This procedure was repeated 25 times and their corresponding averages were considered as a representative value of the group.

RESULTS

Neuronal firing during SPW-Rs

We recorded simultaneously LFP and single unit activity from CA1-CA2 regions and DG in the dorsal HPC, and lSuM with silicon probes in anesthetized rats during theta (THETA) and slow oscillations (SO) epochs (Fig. 1A, SuppFig. 1). Hippocampal and DG neurons were separated into putative excitatory neurons and interneurons. We classified neurons as a function of the way

Table 1. Comparison time of peak firing rate during SPW-Rs between lSuM and CA1 SPW-R-active excitatory neurons (exc = excitatory, act = active)

	Median diff	CI (95%)	p	Test
Time peak firing rate (ms)				
lSuM vs. SPW-R-act CA1 exc	17.7	[3.6, 29.8]	$4.49e^{-3}$	Kruskal–Wallis

their firing activity was changed during SPW-Rs (Fig. 1B). For excitatory neurons, we found that 51% in CA1 (28/55), 20% in CA2 (6/30), 36% in CA3 (12/33), and 12% in DG (2/17) increased their firing during SPWRs ("SPW-R-active neurons"); while 13% in CA1 (7/55) showed a decrease in firing ("SPW-R-suppressed neurons") (Fig. 1B). For putative interneurons, 41% in CA1 (28/68), 75% in CA2 (15/20), 68% in CA3 (15/22), and 63% in DG (7/11) increased their firing, while 18% in CA1 (12/68), and 10% in CA2 (2/20) showed a decrease of their firing rates (Fig. 1B). In the lSuM, 24% of neurons (19/80) showed a significant increase in firing during SPW-Rs ("SPW-R-active neurons") (Fig. 1B). The majority of lSuM neurons (76%) did not display a change in firing during SPW-Rs. Fig. 1D shows four examples of single cell responses during SPW-Rs from lSuM (SPW-R-active and unchanged neurons, left), CA1 SPW-R-active excitatory and CA1 SPW-R-active interneuron (right).

We then looked at the timing of the peak firing rate with respect to the SPW-R peak power (Fig. 1C). The peak firing rate occurred earlier than the SPW-R peak in most SPW-R-active neurons. The earliest firing neurons were the lSuM SPW-R-active neurons. The median time of peak firing was 22 ms before the SPW-R peak. For putative excitatory neurons, the median time of peak firing was 9 ms for CA2 and CA3, and 1.5 ms for CA1 SPW-R-active neurons. For putative interneurons, the median time of peak 7 ms for CA2 and CA3, and 6.5 ms CA1 SPW-R-active cells. The peak firing rate occurred after the SPW-R peak power for only DG SPW-R-active in
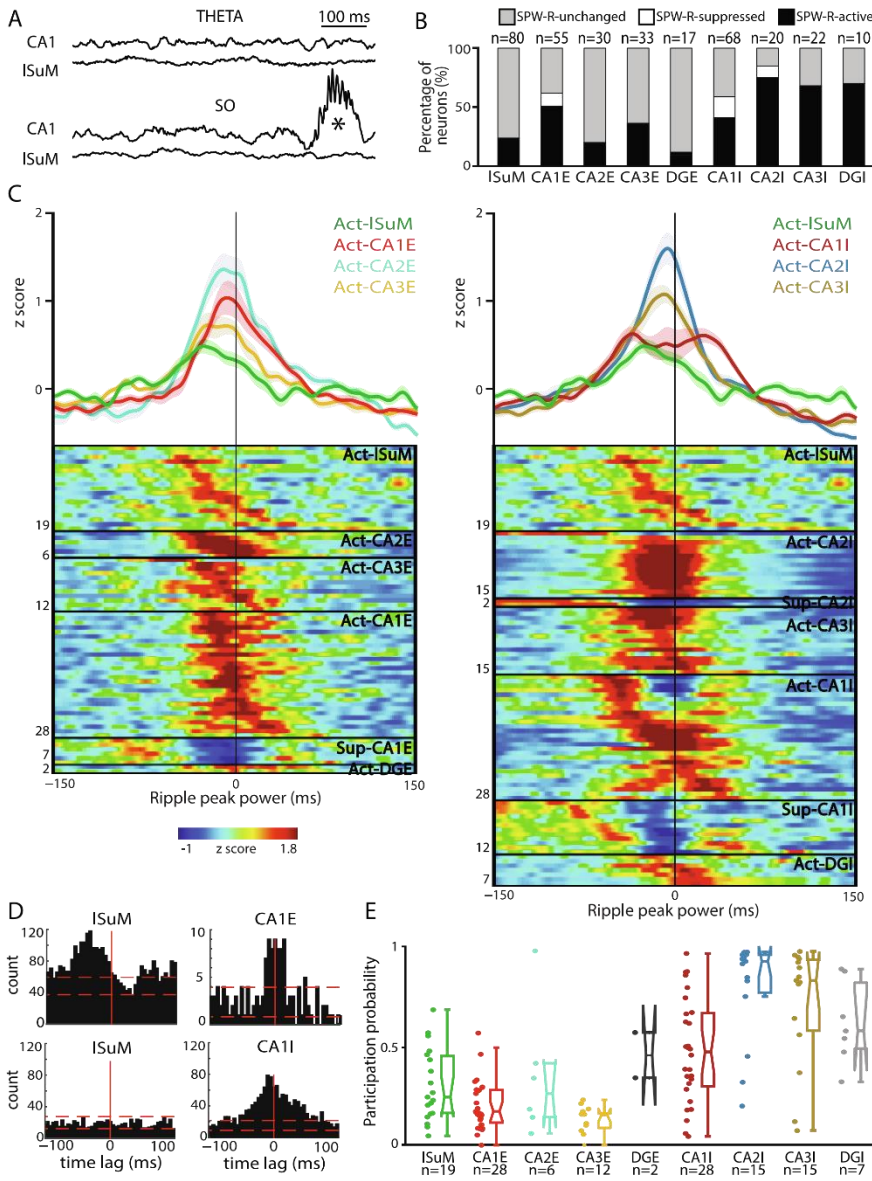
Figure 1. A population of lSuM neurons fire before hippocampal SPW-Rs. (A) LFP traces obtained in the pyramidal layer of CA1 HPC and lSuM during THETA (top) and SO (bottom). Note the ripple during SO (asterisk). (B) Distribution of lSuM, CA1, CA2, CA3 and DG excitatory neurons (E) and interneurons (I) classified as SPW-R-active, SPW-R-suppressed and SPW-R-unchanged. (C) Average (shaded error bars) firing curves per region and Z scored firing rate raster plots centered on SPW-R peak power for SPW-R-active and SPW-R-suppressed neurons. Each row represents the activity of a single neuron. The black vertical line indicates zero-time lag. Numbers to the left of raster plots represent the total number of neurons for every group. Left: Act-lSuM (lSuM SPW-R-active) and putative excitatory neurons including: Act-CA2E (CA2 SPW-R-active), Act-CA3E (CA3 SPWR-active), ActCA1E (CA1 SPW-R-active), Sup-CA1E (CA1 SPW-R-suppressed), and Act-DGE (DG SPW-R-active). Right: Act-lSuM (lSuM SPWR-active) and interneurons including: Act-CA2I (CA2 SPW-R-active), Sup-CA2I (CA2 SPW-R-suppressed), Act-CA3I (CA3 SPW-R-active), ActCA1I (CA1 SPW-R-active), Sup-CA1I (CA1 SPW-R-suppressed), and Act-DGI (DG SPW-R-active). (D) Representative examples of firing patterns from lSuM (SPW-R-active, top left, and unchanged neurons, bottom left), excitatory and interneuron from CA1 (SPW-R-active neurons, top and bottom right). Red vertical line indicates zero-time lag, and red horizontal lines indicate Pointwise line at 99% acceptance level (see Experimental Procedures). Note the peak firing for lSuM SPW-R-active neuron occurring earlier than the peak firing for CA1 excitatory and interneuron. In the example of the CA1 excitatory neuron shown here, the y axis has a different scale due to the neuron's low firing rate. (E) Participation probability defined as the number of SPW-Rs in which a neuron fires divided by the total number of SPW-Rs for lSuM neurons (lSuM), CA1 (CA1E), CA2 (CA2E), CA3 (CA3E), DG (DGE) putative excitatory neurons, and CA1 (CA1I), CA2 (CA2I), CA3 (CA3I), DG (DGI) interneurons. Interneurons show the highest participation probability as compared to lSuM and excitatory neurons. lSuM shows a higher participation probability as compared to CA1 and CA3 excitatory neurons. Filled circles represent the participation probability for each neuron. Statistical boxes for every group represent the median, 25th, 75pth percentiles, and the most extreme data points not considered as outliers. Note the large dispersion of participation probabilities, from 0 to 0.7 for all cell types, and the presence of an important population of CA1, CA2, CA3, and DG interneurons with high (>0.7) participation probabilities.

Table 2. Pair comparisons of participation probability showing significant differences (exc = excitatory, int = interneurons, exc = excitatory)

	Median diff	CI (95%)	p	Test
Participation probability				
lSuM vs. CA1 exc	−0.0732	[−0.282, −0.00162]	0.049	Kruskal-Wallis
lSuM vs. CA1 int	0.23	[0.0393, 0.41]	0.0222	Kruskal-Wallis
lSuM vs. CA2 int	0.404	[0.125, 0.49]	0.019	Kruskal-Wallis
lSuM vs. CA3 exc	−0.0927	[−0.249, −0.00714]	$4.51e^{-3}$	Kruskal-Wallis
lSuM vs. CA3 int	0.591	[0.267, 0.699]	$6.35e^{-4}$	Kruskal-Wallis
lSuM vs. DG int	0.334	[0.094, 0.654]	$3.51e^{-3}$	Kruskal-Wallis
CA1 exc vs. DG exc	0.285	[0.14, 0.411]	0.0306	Kruskal-Wallis
CA3 exc vs. DG exc	0.305	[0.18, 0.447]	0.0276	Kruskal-Wallis
CA1 int vs. CA2 int	0.46	[0.26, 0.599]	$7.01e^{-4}$	Kruskal-Wallis
CA1 int vs. CA3 int	0.363	[0.0663, 0.518]	$9.34e^{-3}$	Kruskal-Wallis

interneurons (9 ms). The peak firing rate was statistically significant between lSuM SPW-R-active neurons and CA1 SPW-R-active excitatory neurons (p = $4.49e^3$, Table 1). The median time of firing suppression peak was 14.5 for CA2 and 10 ms for CA1 SPW-R suppressed interneurons, and 4 ms for CA1 SPW-R suppressed excitatory neurons.

We then calculated the SPW-R participation probability for each SPW-R-active neuron, defined as the number of SPW-Rs in which a neuron fired divided by the total number of SPW-Rs (Fig. 1E, Table 2). CA2 interneurons showed the highest participation probability (median = 0.93), followed by CA3 interneurons (median = 0.83), DG interneurons (median = 0.58), CA1 interneurons (median = 0.47), DG excitatory neurons (median = 0.46), CA2 excitatory neurons (median = 0.26), lSuM neurons (median = 0.24), CA1 excitatory neurons (median = 0.17), and CA3 excitatory neurons (median = 0.15). lSuM neurons fired more frequently than CA1 (p = 0.049), and less frequently than CA1 (p = 0.022), CA2 (p = 0.019), CA3 pyramidal neurons (p = $4.51e^3$), CA3 (p = $6.35e^4$), and DG interneurons (p = $3.51e^3$). CA1 (p = 0.031) and CA3 excitatory neurons (p = 0.028) showed a higher participation probability than DG excitatory neurons. Finally, CA1 interneurons fired less frequently than CA2 (p = $7.01e^4$) and CA3 interneurons (p = $9.34e^3$).

The main difference between CA1/CA2/CA3/DG interneurons and CA1/CA2/CA3/DG excitatory/lSuM neurons stems from the presence of highly participating interneurons showing a high probability (>0.7) to be active during SPW-Rs. Interestingly, the 9 groups have a widespread dispersion of values between 0 (cells that did not participate in SPW-Rs) and 1 (Fig. 1E). Replication studies are necessary to determine whether the cells can be divided into high and low participation probabilities.
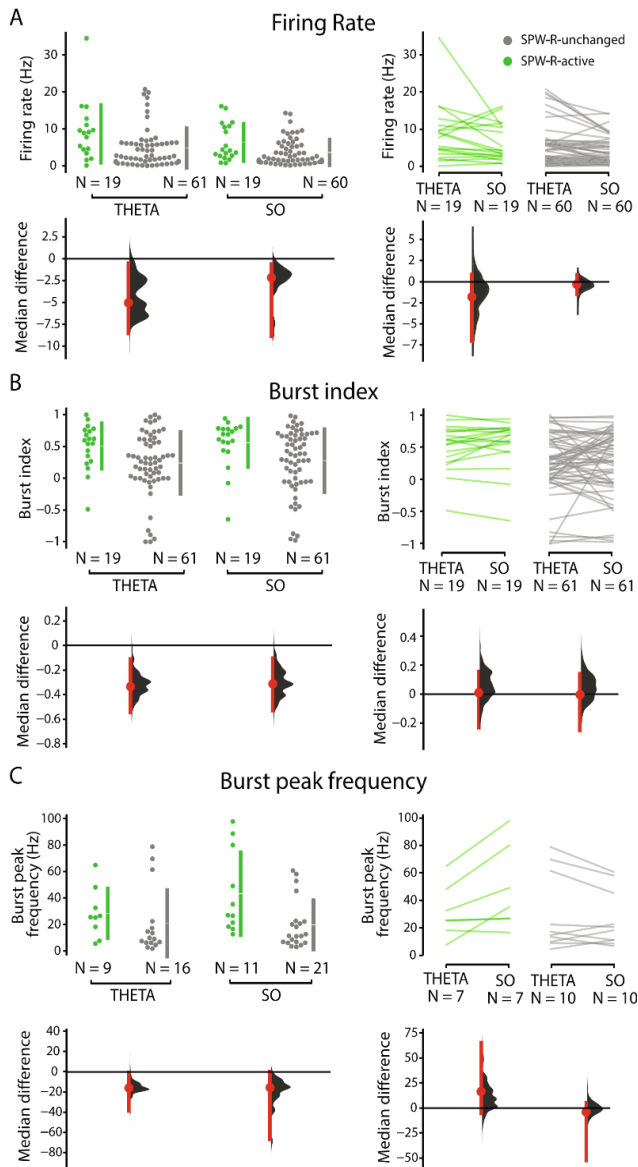
Figure 2 Firing rate and burst parameters for lSuM neurons during theta (THETA) and slow oscillations (SO). (Left) In panels (A–C), upper plot shows values per neuron, represented by dots. Vertical lines to the right of each group represent mean (gap in the lines) ± standard deviation (gapped lines). (Right) In panels (A–C) upper plot shows values per neuron during THETA and SO, represented by lines. The lower plot indicates the median differences between groups. Each median difference is plotted as a bootstrap sampling distribution. Median differences are depicted as dots; 95% confidence intervals are indicated by the ends of the vertical error bars. Firing rate (A left), burst index (B left) and burst peak frequency (C left) differences between SPW-R-active neurons (green) and SPW-R-unchanged neurons (grey). The firing rate and burst index was higher for SPW-R active neurons during THETA and SO. Burst peak frequency was higher for SPW-R-active neurons only during SO. Firing rate (A right), burst index (B right) and burst peak frequency (C right) differences between THETA and SO for SPW-R-active neurons (green) and SPW-R-unchanged neurons (grey). We did not find differences between THETA and SO for either of the neuronal groups. (For interpretation of the references to colour in this figure legend, the reader is referred to the web version of this article.)

Firing properties of lSuM SPW-R-active neurons

We then assessed whether lSuM SPW-R-active neurons had different firing properties as compared to lSuM SPWR-unchanged neurons. To this aim, we compared several parameters characterizing the firing properties of the neurons during THETA and SO states (Table 3).

We found that SPW-R-active neurons had a higher firing rate during THETA and SO (median = 7.77 and 4.17 Hz) than SPW-R-unchanged neurons (median = 2.72 and 1.99 Hz, p = 0.017 for THE and p = 0.0119 for SO, Fig. 2A left, Table 3). Although some SPW-R-active and SPW-R-unchanged neurons increased or decreased their firing rate between THETA and SO, at the population level the median firing rates were not significantly different between THETA (p = 0.107) and SO (p = 0.0247) (Fig. 2A right, Table 3). Using the firing rate and spike properties (asymmetry and width), we did not find an obvious way to distinguish SPW-R-active from SPW-R-unchanged neurons (SuppFig. 2A).

SPW-R-active neurons had a higher bursting activity during THETA and SO (median = 0.59 and 0.69) than SPW-R-unchanged neurons (median = 0.26 and 0.38, p = 0.0151 for THETA, p = 0.0144 for SO, Fig. 2B left, Table 3). Burst indices were similar

between THETA and SO for SPW-R-active (p = 0.314) and SPW-R unchanged neurons (p = 0.544, Fig. 2B right, Table 3).

The peak frequency during the bursting periods (intraburst frequency) of the SPW-R-active neurons was similar to that of SPW-R-unchanged neurons during THETA: median = 25.59 and 9.54 Hz, p = 0.101 (Fig. 2C left, Table 3). However, the intra-burst frequency was higher in SPW-R-active neurons than in SPW-R-unchanged neurons during SO: median = 27.08 and 11.52 Hz, p = 0.00657 (Fig. 2C left, Table 3). We found no significant differences between THETA and SO for either of the neuronal groups (SPW-R-active neurons, p = 0.0425; SPW-R-unchanged neurons, p = 0.285, Fig. 2C right, Table 3). Interestingly, the display of all data seems to indicate the existence of two clusters: one with low and one with high burst peak frequency in all conditions.

Autocorrelation analysis showed that the discharge probability peak occurred earlier during THETA and SO in SPW-R-active (median = 4 and 3 ms) than in SPWR-unchanged neurons (median 55 and 22.4, p = 0.00145 for THETA, p = 5.73e05 for SO, Fig. 3A left, Table 4). This finding indicates that SPW-R-active neurons fire with short inter-spikes intervals, in line with the higher burst activity found in this group, as compared to SPW-R-unchanged neurons. We found a bimodal distribution of the discharge probability for SPW-R-unchanged neurons during SO

Table 3. Pair comparisons of firing properties for lSuM SPW-R-active and unchanged neurons

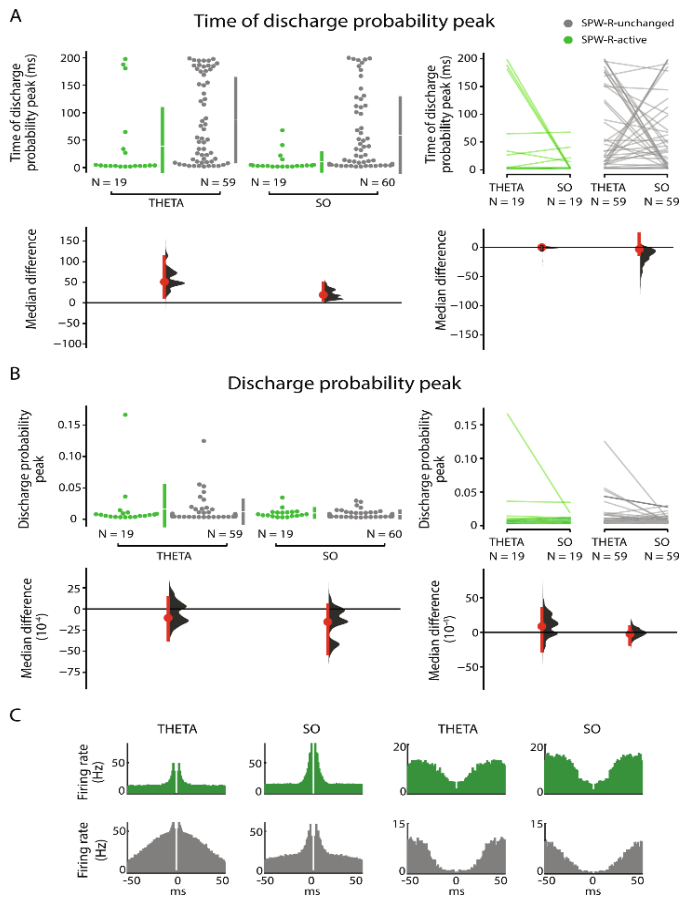|	Median diff	CI (95%)	*p*	Test
Firing rate (Hz)				
SPW-R-active vs. unchanged				
THETA	−5.05	[−8.53, −0.525]	0.017	Kruskal-Wallis
SO	−2.17	[−8.88, −0.624]	0.0119	Kruskal-Wallis
THETA vs. SO				
SPW-R-active	−1.79	[−7.04, 0.856]	0.107	Wilcoxon
SPW-R-unchanged	−0.306	[−1.49, 0.827]	0.0247	Wilcoxon
Burst index				
SPW-R-active vs. unchanged				
THETA	−0.33	[−0.547, −0.112]	0.0151	Kruskal-Wallis
SO	−0.31	[−0.532, −0.104]	0.0144	Kruskal-Wallis
THETA vs. SO				
SPW-R-active	0.0109	[−0.232, 0.154]	0.314	Wilcoxon
SPW-R-unchanged	−0.00227	[−0.25, 0.142]	0.544	Wilcoxon
Peak frequency burst (Hz)				
SPW-R-active vs. unchanged				
THETA	−16.0	[−38.7, −0.964]	0.101	Kruskal-Wallis
SO	−15.6	[−67.4, −0.174]	0.00657	Kruskal-Wallis
THETA vs. SO				
SPW-R-active	16.5	[−5.58, 65.3]	0.0425	Wilcoxon
SPW-R-unchanged	3.94	[−52.6, 5.11]	0.285	Wilcoxon
Phase preference (°)				
SPW-R-active vs. unchanged				
THETA	−6.84	[−44.1, 42.5]	0.768	Kruskal-Wallis
SO	−15.9	[−31.8, −8.9]	0.0112	Kruskal-Wallis
Entrainment strength				
SPW-R-active vs. unchanged				
THETA	−0.00235	[−0.0765, 0.0847]	0.706	Kruskal-Wallis
SO	−0.0496	[−0.0881, 0.0393]	0.836	Kruskal-Wallis

Figure 3 Firing parameters for lSuM neurons during theta (THETA) and slow oscillations (SO). Time of discharge probability peak (A left) and discharge probability peak (B left) differences between SPW-R-active neurons (green) and SPW-R-unchanged neurons (grey). The discharge probability peak occurred earlier in SPW-R-active neurons during THETA and SO. We did not find differences in the discharge probability peak. Time of discharge probability peak (A right) and discharge probability peak (B right) differences between THETA and SO for SPW-R-active neurons (green) and SPW-R-unchanged neurons (grey). We did not find differences between THETA and SO for either of the groups. Same representation as in Fig. 1. (C) Autocorrelograms of two lSuM SPW-R-active (green) and two SPW-R-unchanged neurons (grey) during THETA and SO. Bin size, 1 ms. Note the short latency peak for the two neurons on the left (THETA and SO), while the peak occurs later for the two neurons on the right (THETA and SO). (For interpretation of the references to colour in this figure legend, the reader is referred to the web version of this article.)

(Hartigans' Dip test, p = 0.0473). Although some SPW-R-active and SPW-R-unchanged neurons strongly increased or decreased their time of discharge probability peak between THETA and SO, at the population level there were no significant differences (SPW-R-active neurons, p = 0.375; SPW-R-unchanged neurons, p = 0.049,

Fig. 3A right, Table 4). Interestingly, several populations can be visually identified. The subset of three SPW-R active neurons with a high time of discharge probability during THETA switches to a very low value during SO. For SPW-R-unchanged neurons, three subsets can be identified regarding the difference in time of discharge probability between THETA and SO, neurons displaying a large decrease, a large increase, and no change (Fig. 3A, right). This result further highlights the heterogeneity of lSuM neurons.

The discharge probability peak was not statistically different during THETA and SO between SPW-R-active (median = 0.0069 and 0.0079) and SPW-R-unchanged neurons (median = 0.0059
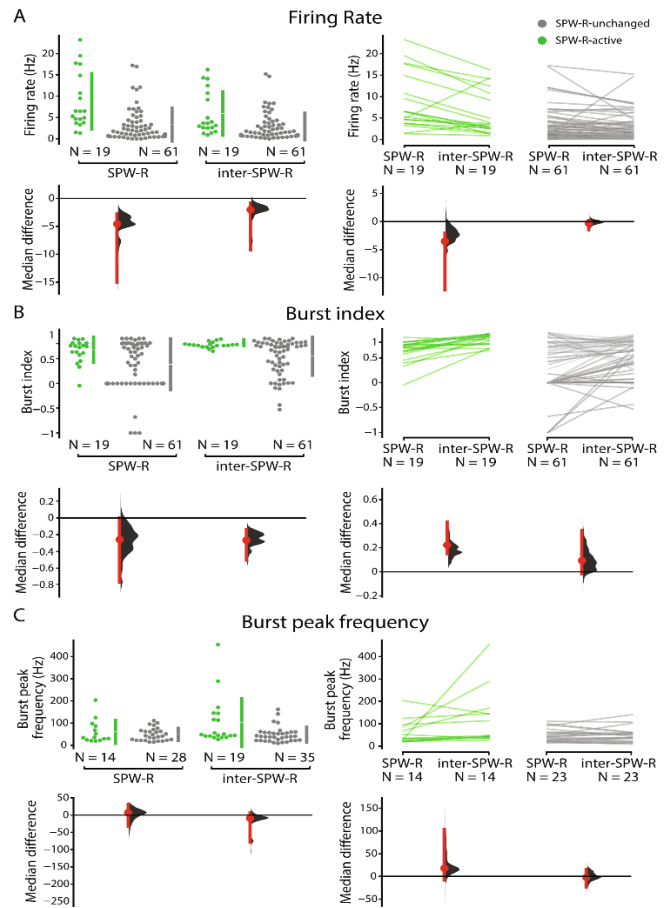

Figure 4 Firing rate and burst parameters for lSuM neurons during SPW-R and inter-SPW-R periods. Firing rate (A left), burst index (B left) and burst peak frequency (C left) differences between SPW-R-active neurons (green) and SPW-R-unchanged neurons (grey) during SPW-R and inter-SPWR periods. The firing rate and burst index was higher for SPW-R-active neurons during SPW-R and inter-SPW-R periods. We did not find differences regarding burst peak frequency for either of the neuronal groups. Firing rate (A right), burst index (B right) and burst peak frequency (C right) differences between SPW-R and inter-SPW-R periods for SPW-R-active neurons (green) and SPW-R-unchanged neurons (grey). Firing rate was higher during SPW-R periods only for SPW-R-active neurons. The burst index was higher during inter-SPW-R periods only for SPW-R-active neurons. We did not find differences regarding burst peak frequency for either of the neuronal groups. Same representation as in Fig. 2. (For interpretation of the references to colour in this figure legend, the reader is referred to the web version of this article.)

and 0.0064, p = 0.82 for THETA, p = 0.297 for SO, Fig. 3B left, Table 4). We did not find differences in discharge probability peak between THETA and SO for either of the two groups (SPW-R-active neurons, p = 0.355; SPW-R-unchanged neurons, p = 0.473, Fig. 3B right, Table 4). The distribution of discharge probability peak was significantly bimodal for SPW-R-unchanged neurons during THETA and SO (Hartigans' Dip test, p = 0.025 and 0.036, respectively). Fig. 3C illustrates four representative autocorrelograms of two lSuM SPW-R-active (green) and two SPW-R-unchanged neurons (grey) during THETA and SO showing short latency peak for the two neurons on the left (THETA and SO), while the peak occurs later for the two neurons on the right (THETA and SO).

Altogether, these results show that lSuM SPW-R active neurons have a greater firing activity as compared to SPW-R-unchanged neurons. We wondered if the higher firing activity during SO was due to a specific increase in firing during SPW-Rs.

Table 4. Pair comparisons of autocorrelation analysis for ISuM SPW-R-active and unchanged neurons

	Median diff	CI (95%)	p	Test
Time of discharge probability peak (ms)				
SPW-R-active vs. unchanged				
THETA	51.0	[13.0, $1.12e^{+2}$]	0.00145	Kruskal-Wallis
SO	19.5	[6.5, 49.0]	$5.73e^{-5}$	Kruskal-Wallis
THETA vs. SO				
SPW-R-active	0.0	[−5, 1.0]	0.375	Wilcoxon
SPW-R-unchanged	−3.0	[−12.0, 23.0]	0.049	Wilcoxon
Discharge probability peak				
SPW-R-active vs. unchanged				
THETA	$-1.1e^{-3}$	[$-3.7e^{-3}$, $1.4e^{-3}$]	0.82	Kruskal-Wallis
SO	$-1.5e^{-3}$	[$-5.3e^{-3}$, $5e^{-4}$]	0.297	Kruskal-Wallis
THETA vs. SO				
SPW-R-active	$8.9e^{-4}$	[$2.8e^{-3}$, $3.5e^{-3}$]	0.355	Wilcoxon
SPW-R-unchanged	$-2.2e^{-4}$	[$-1.8e^{-3}$, $8.6e^{-4}$]	0.473	Wilcoxon

Table 5. Pair comparisons of firing properties for SPW-R and inter-SPW-R periods for ISuM SPW-R-active and unchanged neurons

	Median diff	CI (95%)	p	Test
Firing rate (Hz)				
SPW-R-active vs. unchanged				
SPW-R	−4.57	[−15.1, −2.74]	$5.05e^{-5}$	Kruskal-Wallis
Inter-SPW-R	−2.02	[−9.21, −0.831]	$2.59e^{-3}$	Kruskal-Wallis
SPW-R vs. inter-SPW-R				
SPW-R-active	−3.52	[−5.53, −1.9]	$5.49e^{-3}$	Wilcoxon
SPW-R-unchanged	−0.285	[−0.749, −0.121]	$2.19e^{-3}$	Wilcoxon
Burst index				
SPW-R-active vs. unchanged				
SPW-R	−0.258	[0.768, 0.0]	0.0672	Kruskal-Wallis
Inter-SPW-R	−0.266	[−0.506, −0.141]	$8.99e^{-7}$	Kruskal-Wallis
SPW-R vs. inter-SPW-R				
SPW-R-active	0.22	[0.149, 0.414]	$2.93e^{-4}$	Wilcoxon
SPW-R-unchanged	0.0093	[−0.018 0.34]	$4.23e^{-3}$	Wilcoxon
Burst peak (Hz)				
SPW-R-active vs. unchanged				
SPW-R	7.19	[−33.0, 31.1]	0.689	Kruskal-Wallis
Inter-SPW-R	−8.66	[−77.6, 7.28]	0.0219	Kruskal-Wallis
SPW-R vs. inter-SPW-R				
SPW-R-active	18	[−7.97, 104]	0.0303	Wilcoxon
SPW-R-unchanged	−1.99	[−23.5, 15.4]	0.976	Wilcoxon

We thus tested whether SPW-R-active neurons were also more active outside SPW-R periods. To this aim, we computed the firing rates of both types of neurons during ripples (SPW-R firing rate) and during SO periods excluding ripples times (inter-SPW-R firing rate). SPW-R-active neurons had a higher firing rate during both SPW-R and inter-SPW-R periods than SPW-R unchanged neurons (Fig. 4A left, Table 5). For SPW-R periods: median = 6.5 and 1.93 Hz, p = $5.05e^5$; for inter-SPW-R periods: median = 3.62 and 1.6 Hz, p = 0.00259. Firing rate was higher during SPW-R periods for SPW-R-active neurons (p = 0.00549), and SPW-R-unchanged neurons (p = 0.00219, Fig. 4A right, Table 5).

A higher firing rate for SPW-R-active neurons during SPW-Rs as compared to outside SPW-Rs, or as compared to SPW-R-unchanged neurons, may be due to increased bursting activity. We thus calculated the burst index of both populations during SPW-R and inter SPW-R periods. The burst index was significantly higher for SPW-R-active neurons only during inter-SPW-R periods (Fig. 4B left, Table 5). For SPW-R periods: median = 0.76 for SPW-R-active neurons and 0.5 for SPW-R-unchanged neurons, p = 0.0672. For inter SPW-R periods: median = 0.96 for SPW-R-active neurons and 0.69 for SPW-R-unchanged neurons, p = $8.99e^7$ (Fig. 4B left, Table 5). When comparing burst indices
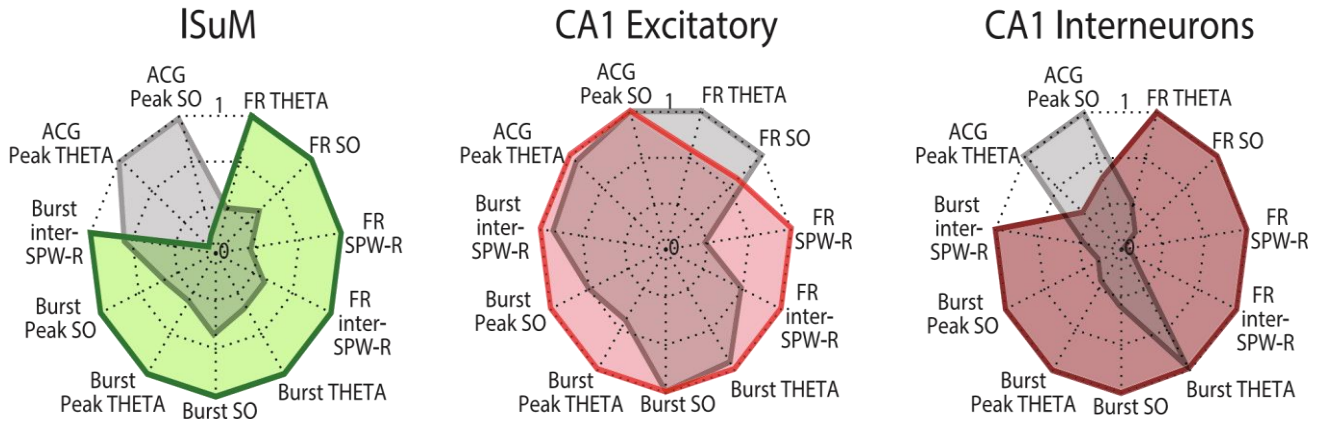
Figure 5 Radar plot of firing parameters showing significant differences (for at least one of the neuronal groups) between SPW-R-active (green) and SPW-R-unchanged (grey) lSuM neurons (left), SPW-R-active (light red) and SPW-R-unchanged (grey) CA1 excitatory neurons (middle), and SPWR-active (dark red) and SPW-R-unchanged (grey) CA1 interneurons (right). Every axis represents a firing parameter and its corresponding mean value for SPW-R-active and SPW-R-unchanged neurons. All values corresponding to the same group are connected to form a polygon. All values are normalized. The relative position and angle of the axes are not informative. FR THETA and FR SO: firing rate during theta (THETA) and slow oscillation (SO), FR SPW-R and inter-SPW-R: firing rate during SPW-R and inter-SPW-R periods, Burst THETA and SO: burst index during THETA and SO, Burst Peak THETA and SO: burst peak frequency during THETA and SO, Burst inter-SPW-R: burst index during inter-SPW-R periods, ACG Peak THETA and SO: time of discharge probability peak during THETA and SO. The distinct shape of the polygons illustrates the differences between SPW-R-active and SPW-R-unchanged neurons according to their firing properties. (For interpretation of the references to colour in this figure legend, the reader is referred to the web version of this article.)

between SPW-R and inter-SPW-R periods, we found a higher burst index during inter-SPW-R periods only for the SPW-R-active population (p = 2.93e3, Fig. 4B right, Table 5).

Regarding intra-burst frequency, we found no significant differences either for SPW-R or for inter- SPW-R periods between SPW-R-active (median = 35.09 and 47.92 Hz) and SPW-R-unchanged neurons (median = 42.29 and 39.26 Hz, p = 0.689 for SPW-R periods, p = 0.0219 for inter-SPW-R periods (Fig. 4C left, Table 5). We did not find significant differences when comparing SPW-R and inter-SPW-R periods (p = 0.0303 for SPW-R-active neurons, p = 0.976 for SPW-R-unchanged neurons, Fig. 4C right, Table 5).

We then examined how neuronal firing was modulated by the ongoing brain oscillation. Most of lSuM neurons were entrained by the ongoing oscillatory activity. Specifically, 96.2% (77/80) were entrained during THETA epochs; and 98.7% (79/80) during SO epochs, p < 0.05, Rayleigh test, Supl Fig. 2B, Table 3). Whereas SPW-R-active and SPW-R-unchanged neurons did not display any difference in their theta phase preference (median = 78.13 and 170.47, respectively, p = 0.768), SPW-R-active neurons fired later during the trough of the slow oscillation median = 228.01) as compared to SPW-R-unchanged neurons during SO (median = 212.97, p = 0.0112) (Supl Fig. 2C and 2D, Table 3). Although we found significant differences between the two neuronal populations during SO, similar distributions of the individual values point to a weak significant difference (Supl Fig. 2D, Table 3). We did not find differences for the strength of the entrainment between the two populations either for THETA or for SO (median = 0.17 and 0.15 for THETA, p = 0.71; median = 0.21 and 0.19 for SO, p = 0.84).

We similarly analyzed CA1 excitatory and interneurons, which results are presented in Tables S2–7. In summary, we found that firing patterns were significantly different between SPW-R-active and SPW-R-unchanged CA1 interneurons, but

much less so as compared to CA1 excitatory neurons. Together, these results show that it is possible to clearly separate SPW-R-active from SPW-R-unchanged lSuM neurons and CA1 interneurons on the basis of their firing properties, while this separation is less clear for CA1 excitatory neurons (Fig. 5).

Correlation between lSuM firing and SPW-R parameters

Finally, we examined whether the firing of lSuM SPW-R active neurons was correlated with SPW-R properties like their duration, peak power and frequency (total number of ripples = 1618). We found a negative but weak correlation between SPW-R-active neurons firing and SPW-R duration (r = 0.12, p = 7.7597e7, Pearson correlation, Fig. 6A, Table 6), and SPW-R frequency (r = 0.07, p = 0.002, Pearson correlation, Fig. 6C, Table 6). Regarding SPW-R peak power, SPW-R-active neurons showed a positive correlation (r = 0.41, p = 7.5342e68, Pearson correlation, Fig. 6B, Table 6). These results indicate that the firing of SPWR-active neurons during SPW-Rs depends on SPW-R parameters. This neuronal group is more active during high peak power SPW-Rs.
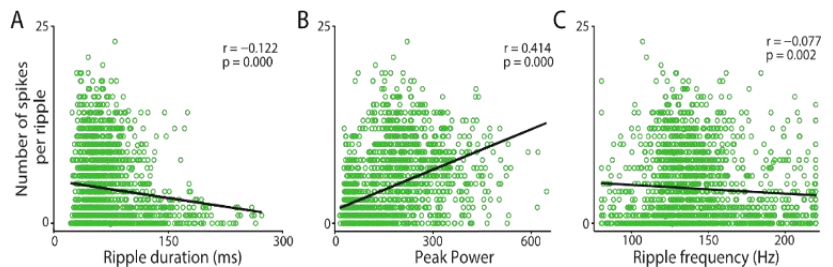

Figure 6 Correlation between ripples parameters and the firing of lSuM SPW-R-active neurons firing during ripples. Each circle indicates the number of spikes per ripple and its corresponding ripple parameter. The correlation coefficient (Pearson correlation) and p value are shown. (A) Ripple duration and number of spikes per ripple are negatively correlated. (B) Ripple peak power and number of spikes per ripple are positively correlated. (C) Ripple frequency and number of spikes per ripple are negatively correlated.

DISCUSSION

The interaction between the SuM and the HPC has mostly been studied in the context of hippocampal theta oscillations since the SuM is connected with other nuclei involved in theta generation, such as the reticular formation and the septum (Green and Arduini, 1954). In the present study we characterized neuronal activity in the lSuM during both theta and slow oscillation dominated states and its interaction with hippocampal SPW-Rs in anesthetized rats. We found SPW-R associated firing in a population of lSuM neurons. The latter increased their firing prior to SPW-R peak power and prior CA1 excitatory cells. They showed distinct firing properties and tended to fire more during high peak power ripples. These findings suggest the existence of an interaction between lSuM and hippocampal SPW-Rs and raise questions about the causality of this interaction and its functional significance.

We demonstrate that a population of lSuM neurons increase their firing 22 ms before dorsal CA1 SPW-Rs, which suggests coordinated activity between both regions. However, the lSuM is not directly connected to dorsal CA1 HPC (Vertes, 1992; Magloczky et al., 1994), where SPW-Rs were recorded. This lSuM-SPW-R interaction may be explained by indirect connections between lSuM and dorsal CA1 (Supp. Fig. 3). The lSuM innervates *stratum oriens* and pyramidal layer of dorsal CA2 and CA3 (Vertes, 1992; Magloczky et al., 1994), hippocampal regions postulated to generate SPW-Rs (Csicsvari et al., 2000; Oliva et al., 2016). The lSuM also sends afferents to the DG, which, in turn, connects to CA2 (Vertes and McKenna, 2000). Sullivan et al. (2011) proposed that DG inputs modulate the occurrence of SPW-Rs as there is a positive correlation between dentate gamma power and the frequency of SPW-R occurrence. The lSuM has an excitatory effect on the dorsal DG (Carre and Harley, 1991; Nakanishi et al., 2001) but also an inhibitory effect (Segal, 1979; Mizumori et al., 1989), likely due to the dual glutamatergic and GABAergic phenotype of lSuM projections to the DG (Soussi et al., 2010). Both excitatory and inhibitory lSuM projections to the DG could be responsible for an indirect influence on SPW-Rs. Moreover, CA2, CA3 and the DG connect dorsal CA1 (Amaral and Witter, 1989), which may also explain the origin of the CA1 SPW-R-associated neuronal firing found in the lSuM (Supl Fig. 3).

is in accordance with the higher bursting activity of this population. SPW-R-active neurons are also more active than SPW-R-unchanged neurons during SPW-R periods, which is in accordance with their increase of firing during SPW-Rs. The fact that we also found differences between these neuronal groups during inter SPW-R periods demonstrates the existence of two functionally distinct neuronal populations in lSuM: SPWR-active neurons characterized by a higher excitability during THETA and SO and an increase of firing during SPW-Rs, and SPW-R-unchanged neurons characterized by a lower activity and no changes of firing during SPWRs. Apart from the SPW-R modulation criterion, we could not identify other morphological

The lSuM SPW-R related firing could also be explained by their reciprocal connections with the septum complex. The lSuM sends afferents to the medial and lateral septum contacting both excitatory cells and interneurons; and at least 25% of these projections connect to the dorsal HPC as well (Leranth and Kiss, 1996; Borhegyi et al., 1998; Kiss et al., 2000). Furthermore, Unal et al. (2018) described two neuronal populations in the medial septum showing SPW-R related activity: one population suppressed its firing during SPWRs while the other population was activated. Finally, the septum sends projections to hippocampal interneurons (Freund and Antal, 1988). These results raise the possibility of an indirect pathway from the SuM to CA1 via the septum, which may explain the lSuM SPW-R related firing identified in the present work.

The firing of lSuM activated neurons precedes hippocampal neuronal firing during SPW-Rs. It would be tempting to propose that the lSuM may act as a hippocampal driver. However, caution is in order. If SPW-Rs are activities emerging from a large network of brain regions, early firing may just mark the onset of the emergence of the event, without necessarily implying causality. Nevertheless, lSuM firing is followed by SPWR-active CA1 excitatory neurons, which suggests a modulation of CA1 excitatory activity by lSuM.

lSuM firing is also followed by SPW-R-active CA1 interneurons, CA2, CA3 and DG excitatory neurons and interneurons, as shown by the median timing of peak firing rate. However, differences between lSuM and these neurons were not significant, which could be due to a low number of neurons recorded in CA1, CA2, CA3 and DG. More experiments are needed to establish reliable conclusions. Nevertheless, these results suggest that lSuM could modulate the firing of CA1, CA2, CA3 and DG during SPW-Rs as well. Circuit manipulation experiments using optogenetic tools are now needed to investigate in further detail the role of lSuM in SPW-R and, hippocampal and DG firing modulation.

lSuM SPW-R-active neurons show different firing properties as compared to lSuM SPW-R-unchanged neurons. SPW-R-active neurons discharge more frequently and tend to burst during both THETA and SO states. The intra-burst frequency is also higher for SPWR-active neurons during SO. The discharge probability peak from the autocorrelogram occurs earlier during both THETA and SO for SPW-R-active neurons, which

or physiological ways to distinguish lSuM neurons, in terms of anatomical distribution and waveform parameters, respectively (SuppFig. 2A). Enhancer gene-driven technology may help to identify different cell types in the lSuM and control them (Nair et al., 2020). Based on the anatomo-functional organization, we hypothesize that SPW-R-active neurons correspond to SuM projections connecting both medial septum and dorsal HPC (Borhegyi et al., 1998), which are likely to be glutamatergic/aspartatergic (Kiss et al., 2000). These three areas, lSuM, medial septum and dorsal HPC, could be part of a circuit involved in SPW-R modulation.

In the hippocampus, 80% of the neurons display a change in firing during SPW-R-s (Oliva et al., 2016). In the present work, we found between 20% and 70% depending upon the hippocampal cell type. The discrepancy is unlikely due to a sampling bias as we recorded a large number of SPW-Rs (between 109 and 675 per animal), which is consistent with the number of ripples analyzed in previous studies (Unal et al., 2018). A lower percentage of SPW-R active neurons may be due to anesthesia. Of note, Ylinen et al. (1995) reported an even lower number (10%) of CA1 pyramidal layer neurons entrained by SPW-Rs. Even if anesthesia affects global brain state dynamics and neuronal firing, the basic rules underlying the organization of neuronal firing at the microcircuit level are similar during natural sleep and anesthesia (Clawson et al., 2019). The proportion of SPW-R active lSuM neurons may be larger during natural sleep.

SPW-Rs are considered an important mechanism to transfer memory from hippocampus to neocortex (Buzsáki, 2015). The fact that lSuM firing is coordinated with SPW-Rs suggests a role of this hypothalamic nucleus in memory. Supporting this hypothesis, Shahidi et al. (2004) found deficits in consolidation of a passive avoidance task when reversible inactivation of SuM was performed in rats. In addition, evidence of memory impairment after electrolytic lesion or inactivation of the SuM has been shown (Aranda et al., 2006; 2008). Consistently with these findings, Ito et al. (2009) found an increase of c-fos expression in the SuM after exploring a novel environment. Moreover, Renouard et al. (2015) showed that projections from the SuM and the claustrum are responsible for the FOS overexpression found in the cortex during REM sleep hypersomnia, suggesting an involvement of the SuM in cognitive processing. Ito et al. (2018) demonstrated the role of the SuM in spatial navigation by showing an impairment of trajectory representation in nucleus reuniens and CA1 following SuM inactivation, although the animal's behavioral performance was not affected. Despite these works point to the role of the SuM in memory, none studied memory-related processes during sleep, the period during which memory consolidation is supposed to occur (Rasch and Born, 2013). Studying the neuronal activity of the SuM and the HPC during the sleep period following the learning of a task would help us to understand if the lSuM-hippocampal interaction during SPW-Rs we describe here reflects memory processes.

DECLARATION OF INTERESTS

None.

REFERENCES

Amaral DG, Witter MP (1989) The three-dimensional organization of the hippocampal formation: a review of anatomical data. Neuroscience 31:571–591.

Amarasingham A, Harrison MT, Hatsopoulos NG, Geman S (2012) Conditional modeling and the jitter method of spike resampling. J Neurophysiol 107:517–531.

Aranda L, Begega A, Sánchez-Ló´pez J, Aguirre JA, Arias JL, Santı´n LJ (2008) Temporary inactivation of the supramammillary area impairs spatial working memory and spatial reference memory retrieval. Physiol Behav 94:322–330.

Aranda L, Santı´n LJ, Begega A, Aguirre JA, Arias JL (2006) Supramammillary and adjacent nuclei lesions impair spatial working memory and induce anxiolitic-like behavior. Behav Brain Res 167:156–164.

Barthó P, Hirase H, Monconduit L, Zugaro M, Harris KD, Buzsáki G (2004) Characterization of neocortical principal cells and interneurons by network interactions and extracellular features. J Neurophysiol 92:600–608.

Borhegyi Z, Maglóczky Z, Acsády L, Freund TF (1998) The supramammillary nucleus innervates cholinergic and GABAergic neurons in the medial septum-diagonal band of Broca complex. Neuroscience 82:1053–1065.

Buzsáki G (2015) Hippocampal sharp wave-ripple: a cognitive biomarker for episodic memory and planning. Hippocampus 25:1073–1188.

Buzsáki G, Lai-Wo SL, Vanderwolf CH (1983) Cellular bases of hippocampal EEG in the behaving rat. Brain Res Rev 6:139–171.

Buzsáki G, Schomburg EW (2015) What does gamma coherence tell us about inter-regional neural communication? Nat Neurosci 18:484–489.

Carre GP, Harley CW (1991) Population spike facilitation in the dentate gyrus following glutamate to the lateral supramammillary nucleus. Brain Res 568:307–310.

Clawson W, Vicente AF, Ferraris M, Bernard C, Battaglia D, Quilichini PP (2019) Computing hubs in the hippocampus and cortex. Sci Adv 5:eaax4843.

Csicsvari J, Hirase H, Czurko A, Buzsáki G (1998) Reliability and state dependence of pyramidal cell-interneuron synapses in the hippocampus: an ensemble approach in the behaving rat. Neuron 21:179–189.

Csicsvari J, Hirase H, Mamiya A, Buzsáki G (2000) Ensemble patterns of hippocampal CA3-CA1 neurons during sharp waveassociated population events. Neuron 28:585–594.

Diekelmann S, Born J (2010) The memory function of sleep. Nat Rev Neurosci 11:114–126.

Dragoi G, Carpi D, Recce M, Csicsvari J (1999) Interactions between hippocampus and medial septum during sharp waves and theta oscillation in the behaving rat. J Neurosci 19:6191–6199.

Ferraris M, Ghestem A, Vicente AF, Nallet-Khosrofian L, Bernard C, Quilichini PP (2018) The nucleus reuniens controls long-range hippocampo-prefrontal gamma synchronization during slow oscillations. J Neurosci 38:3058–3117.

Freund TF, Antal M (1988) GABA-containing neurons in the septum control inhibitory interneurons in the hippocampus. Nature 336:170–173.

Fujisawa S, Amarasingham A, Harrison MT, Buzsáki G (2008) Behavior-dependent shortterm assembly dynamics in the medial prefrontal cortex. Nat Neurosci 11:823–833.

Girardeau G, Inema I, Buzsáki G (2017) Reactivations of emotional memory in the hippocampus-amygdala system during sleep. Nat Neurosci 20:1634–1642.

Green JD, Arduini AA (1954) Hippocamapal electrical activity in arousal. J Neurophysiol 17:533–557.

Grundy D (2015) Principles and standards for reporting animal experiments in The Journal of Physiology and Experimental Physiology. Exp Physiol 100:755–758.

Harris KD, Henze DA, Csicsvari J, Hirase H, Buzsaki G (2000) Accuracy of tetrode spike separation as determined by simultaneous intracellular and extracellular measurements. J Neurophysiol 84:401–414.

Hazan L, Zugaro M, Buzsáki G (2006) Klusters, NeuroScope, NDManager: a free software suite for neurophysiological data processing and visualization. J Neurosci Methods 155:207–216.

Ito M, Shirao T, Doya K, Sekino Y (2009) Three-dimensional distribution of Fos-positive neurons in the supramammillary nucleus of the rat exposed to novel environment. Neurosci Res 64:397–402.

Ito HT, Moser EI, Moser MB (2018) Supramammillary nucleus modulates spike-time coordination in the prefrontal-thalamohippocampal circuit during navigation. Neuron 99:576–587.

Katona L, Lapray D, Viney TJ, Oulhaj A, Borhegyi Z, Micklem BR, Klausberger T, Somogyi P (2014) Sleep and movement differentiates actions of two types of somatostatin expressing GABAergic interneuron in rat hippocampus. Neuron 82:872–8867.

Kirk IJ, McNaughton N (1993) Mapping the differential effects of procaine on frequency and amplitude of reticularly elicited hippocampal rhythmical slow activity. Hippocampus 3:517–525.

Kiss J, Csáki Á , Bokor H, Shanabrough M, Leranth C (2000) The supramammillo-hippocampal and supramammillo-septal glutamatergic/aspartatergic projections in the rat: a combined [3H]D-aspartate autoradiographic and immunohistochemical study. Neuroscience 97:657–669.

Kocsis B, Vertes RP (1994) Characterization of neurons of the supramammillary nucleus and mammillary body that discharge rhythmically with the hippocampal theta rhythm in the rat. J Neurosci 14:7040–7052.

Lee AK, Wilson MA (2002) Memory of sequential experience in the hippocampus during slow wave sleep. Neuron 36:1183–1194.

Leranth C, Kiss J (1996) A population of supramammillary area calretinin neurons terminating on medial septal area cholinergic and lateral septal area calbindincontaining cells are aspartate/ glutamatergic. J Neurosci 16:7699–7710.

Magloczky Z, Acsady L, Freund TF (1994) Principal cells are the postsynaptic targets of supramammillary afferents in the hippocampus of the rat. Hippocampus 4:322–334.

Maingret N, Girardeau G, Todorova R, Goutierre M, Zugaro M (2016) Hippocampo-cortical coupling mediates memory consolidation during sleep. Nat Neurosci 19.

Manouze H, Ghestem A, Poillerat V, Bennis M, Ba-Mhamed S, Benoliel JJ, Becker C, Bernard C (2019) Effects of single cage housing on stress, cognitive, and seizure parameters in the rat and mouse pilocarpine models of epilepsy. eNeuro 6(4).

Mizumori SJ, McNaughton BL, Barnes CA (1989) A comparison of supramammillary and medial septal influences on hippocampal field potentials and single-unit activity. J Neurophysiol 61:15–31.

Nair RR, Blankvoort S, Lagartos MJ, Kentros CG (2020) Enhancer-driven gene expression (EDGE) enables the generation of viral vectors specific to neuronal subtypes. iScience:100888.

Nakanishi K, Saito H, Abe K (2001) The supramammillary nucleus contributes to associative EPSP-spike potentiation in the rat dentate gyrus in vivo. Eur J Neurosci 13:793–800.

Navarrete M, Alvarado-Rojas C, Le Van Quyen M, Valderrama M (2016) RIPPLELAB: a comprehensive application for the detection, analysis and classification of high frequency oscillations in electroencephalographic signals. PLoS One 11.

Oliva A, Fernández-Ruiz A, Buzsáki G, Berényi A (2016) Role of hippocampal CA2 region in triggering sharp-wave ripples. Neuron:1–14.

Pan W-X, McNaughton N (2004) The supramammillary area: its organization, functions and relationship to the hippocampus. Prog Neurobiol 74:127–166.

Pennartz CMA (2004) The ventral striatum in off-line processing: ensemble reactivation during sleep and modulation by hippocampal ripples. J Neurosci 24:6446–6456.

Pignatelli M, Beyeler A, Leinekugel X (2012) Neural circuits underlying the generation of theta oscillations. J Physiol Paris 106:81–92.

Quilichini P, Sirota A, Buzsáki G (2010) Intrinsic circuit organization and theta-gamma oscillation dynamics in the entorhinal cortex of the rat. J Neurosci 30:11128–11142.

Rasch B, Born J (2013) About sleep's role in memory. Physiol Rev 93:681–766.

Renouard L, Billwiller F, Ogawa K, Clement O, Camargo N, Abdelkarim M, Gay N, Scote-Blachon C, Toure R, Libourel P,
Ravassard P, Salvert D, Peyron C, Claustrat B, Leger L, Salin P, Malleret G, Fort P, Luppi P-H (2015) The supramammillary nucleus and the claustrum activate the cortex during REM sleep. Sci Adv 1:e1400177.

Royer S, Zemelman BV, Losonczy A, Kim J, Chance F, Magee JC, Buzsáki G (2012) Control of timing, rate and bursts of hippocampal place cells by dendritic and somatic inhibition. Nat Neurosci 15:769–775.

Segal M (1979) A potent inhibitory monosynaptic hypothalamohippocampal connection. Brain Res 162:137–141.

Shahidi S, Motamedi, Fereshteh, Naghdi N (2004) Effect of reversible inactivation of the supramammillary nucleus on spatial learning. Behav Brain Res 1026:267–274.
Sohal VS, Huguenard JR (2005) Inhibitory coupling specifically generates emergent gamma oscillations in diverse cell types. Proc Natl Acad Sci U S A 102:18638–18643. Soussi R, Zhang N, Tahtakran S, Houser CR, Esclapez M (2010) Heterogeneity of the supramammillary-hippocampal pathways: evidence for a unique GABAergic neurotransmitter phenotype and regional differences. Eur J Neurosci 32:771–785.

Sullivan D, Csicsvari J, Mizuseki K, Montgomery S, Diba K, Buzsaki G (2011) Relationships between hippocampal sharp waves, ripples, and fast gamma oscillation: influence of dentate and entorhinal cortical activity. J Neurosci 31:8605–8616.

Unal G, Crump MG, Viney TJ, E´ ltes T, Katona L, Klausberger T, Somogyi P (2018) Spatiotemporal specialization of GABAergic septo-hippocampal neurons for rhythmic network activity. Brain Struct Funct 223:2409–2432.

Vertes RP (1992) PHA-L analysis of projections from the supramammillary nucleus in the rat. J Comp Neurol 326:595–622.

Vertes RP, McKenna JT (2000) Collateral projections from the supramammillary nucleus to the medial septum and hippocampus. Synapse 38:281–293.

Ylinen A, Bragin A, Nádasdy Z, Jando´ G, Szabo´ I, Sik A, Buzsáki G (1995) Sharp wave associated high-frequency oscillation (200 Hz) in the intact hippocampus: network and intracellular mechanisms.
J Neurosci 15:30–46.